PERGAMON

International Journal of Solids and Structures 40 (2003) 5081–5095

INTERNATIONAL JOURNAL OF SOLIDS and STRUCTURES

www.elsevier.com/locate/ijsolstr

Secondary flows of viscoelastic liquids in straight tubes

Mario F. Letelier [a,*], Dennis A. Siginer [b]

[a] *Departamento de Ingeniería Mecánica, Universidad de Santiago de Chile, Casilla 10233, Santiago, Chile*
[b] *College of Engineering, Wichita State University, 1845 Fairmount, Wichita, KS 67260-0044, USA*

Received 13 September 2002; received in revised form 30 January 2003

Abstract

The unsteady flow of the Green–Rivlin fluids in straight tubes of arbitrary cross-section driven by a pulsating pressure gradient is investigated. The non-linear constitutive structure defined by a series of nested integrals over semi-infinite time domains is perturbed simultaneously with the boundary of the base flow through a novel approach to domain mapping. The dominant primary component of the flow, the longitudinal field, and the much weaker transversal field arise at the first and the second orders of the analysis, respectively. The secondary field is driven by first-order terms stemming from the linearly viscoelastic longitudinal flow at the first order. The domain mapping technique employed yields a continuous spectrum of unconventional closed cross-sectional shapes. We present longitudinal velocity profiles and transversal time-averaged, mean secondary flow streamline patterns for a specific fluid and for representative cross-sectional shapes in the spectrum the triangular, square and hexagonal shapes.

Keywords: Viscoelastic; Flow; Secondary; Arbitrary; Shape

1. Introduction

The behavior of non-Newtonian liquids when subjected to a periodic forcing oscillating about a non-zero mean in circular pipes has been the subject of numerous investigations starting with Barnes et al. (1971) because it arises often in applications, and due to its inherent fundamental appeal as a tool to test the predictive power of constitutive equations and as a potential rheometer. Predicting the flow behavior in particular when the driving pressure gradient pulsates with large amplitudes remains a challenge. The interest in this flow class with fluids which exhibit elasticity finds more emphasis because of the enhancement effect, that is a net increase in the mean flow rate over that corresponding to the steady flow driven by the mean pressure gradient of the pulsating gradient driving the quasi-unsteady flow. This net increase can be substantial depending on the flow parameters as demonstrated by Barnes et al. (1971). The point should be made that quantitative prediction of the flow enhancement with viscoelastic liquids remains elusive for the popular differential type constitutive equations in use at this time. Single integral models with strain-rate memory type kernels seem to predict some experimental facts better in the context of time-periodic flows. In this vein a

* Corresponding author. Fax: +56-2-6816147.
E-mail address: mletelie@lauca.usach.cl (M.F. Letelier).

0020-7683/$ - see front matter © 2003 Elsevier Ltd. All rights reserved.
doi:10.1016/S0020-7683(03)00256-7

nested integral series representation over semi-infinite time domains for the extra-stress functional of a fading memory viscoelastic fluid has been introduced and used by Siginer (1991a) and Siginer and Valenzuela-Rendón (1993) in a series of papers to study this phenomena in circular pipes with better success than differential type and single integral constitutive equations with strain or strain-rate memory type kernels.

So far all the work done in this area is related to flow in circular pipes. In a series of papers (Letelier et al., 2002; Siginer and Letelier, 2002), the authors studied for the first time pulsating pressure gradient driven flow in pipes with cross-sectional shapes other than circular using the nested integral series representation over semi-infinite time domains for the extra-stress functional. The primary longitudinal flow is studied in depth in Letelier et al. (2002) and the secondary flow field is investigated in Siginer and Letelier (2002). It is well known that deviations from the circular shape do not alter the null transversal field in laminar flow for linear fluids although weak secondary flow structures have been observed in the turbulent flow of Newtonian fluids in non-circular tubes early in the century by Nikuradse (1930). In the case of non-linear fluids even slight deviations from circular shape give rise to secondary flows the strength of which albeit weak increases with increasing deviations from the circular shape. Even though the magnitude of the secondary flows does not exceed at most 5% of the magnitude of the primary longitudinal flow secondary flows have been shown to be the dominant mechanism behind the experimentally observed heat transfer enhancement phenomena with viscoelastic fluids in steady laminar flow (Hartnett and Kostic, 1985, 1989; Gao and Hartnett, 1993, 1996). There is also experimental evidence that secondary flows practically do not require an increase in the energy input to drive the flow, that is an increase of the steady pressure gradient. Heat transfer characteristics of viscoelastic fluids in steady laminar flow in rectangular straight tubes is still very much an open question let alone heat transfer characteristics both in steady and quasi-unsteady flow in tubes other than rectangular such as triangular, hexagonal, etc. To our knowledge even the heat transfer phenomena in steady laminar flow of linear fluids in tubes of cross-sectional shape other than rectangular has not been investigated with the obvious exception of round pipes. When it comes to viscoelastic fluids the field is almost virgin territority.

A mathematically rigorous and general theorem concerning the existence of secondary flows in straight tubes of arbitrary cross-section was proved by Fosdick and Serrin (1973). They showed that unless the cross-section of the tube is circular or an annulus between two concentric circles a simple fluid cannot undergo a steady rectilinear motion in a straight tube whose cross-section is a bounded and connected set assuming that the material functions satisfy appropriate analyticity and monotonicity conditions and that they are not proportional for small shear rates. The conditions for steady rectilinear flow of a viscoelastic fluid in tubes of arbitrary cross-section were also previously deduced by Oldroyd (1965). Rectilinear flow can occur in a straight tube of arbitrary cross-section if any one of the following three conditions are met; if the second normal stress difference is zero or both the apparent viscosity and the second normal stress coefficient are constant or if they are proportional. In the latter case the magnitude of the departure of the second normal stress coefficient from a constant multiple of the apparent shear viscosity determines the strength of the secondary flow. Thus fluids which obey the upper convected Maxwell or the Oldroyd—B models and some versions of the Phan-Thien–Tanner model will not develop secondary flows and will display rectilinear particle pathlines when flowing in tubes of cross-section other than circular. If none of the above conditions is met a secondary flow occurs in the transversal plane which causes the particles to follow a spiraling path down the tube. In the case of Maxwell and Oldroyd—B constitutive structures the second normal stress difference $N_2(\kappa^2)$ is zero. Some versions of the Phan-Thien–Tanner model produce a constant second normal stress coefficient $\Psi_2(\kappa) = N_2(\kappa^2)/\kappa^2$ and constant apparent viscosity $\eta'(\kappa)$, other versions predict $\Psi_2(\kappa^2) = m\eta'(\kappa)$ where m is a coefficient of proportionality.

This paper summarizes the recent efforts of the authors to contribute to the prediction of the primary and secondary flows of viscoelastic fluids in conduits of arbitrary shape in quasi-unsteady flow driven by a pulsating pressure gradient. It also puts previous results (Letelier et al., 2002; Siginer and Letelier, 2002) in a more general perspective developed through an ongoing analysis of Phan-Thien–Tanner fluids under

comparable dynamic conditions. Some general kinematic flow structures, common to flows of fluids with different viscoelastic constitutive equations, are presented herein (Letelier et al., 2001). Forthcoming papers will continue this line of investigation for steady flow when the fluid is characterized by differential type constitutive equations, in particular by Phan-Thien–Tanner type of equations, and will look at the heat transfer issues with non-linear fluids in tubes of non-circular shape.

2. Mathematical analysis

The field equations and the boundary conditions read as

$$\rho\frac{\mathrm{D}\mathbf{u}}{\mathrm{D}t}=-\nabla\phi+\nabla\cdot\mathbf{S},\quad \nabla\cdot\mathbf{u}=0\quad \text{in } D,\quad D=\left\{(r,\theta,z):0\leqslant r\leqslant r\,|_{\partial D},0\leqslant\theta<2\pi,-\infty<z<\infty\right\},$$
$$\mathbf{u}\left(r\,|_{\partial D},\theta,z,t\right)=0,\quad \mathbf{u}(0,\theta,z,t)<\infty. \tag{1}$$

The forcing function and the velocity field satisfy

$$\phi_{,z}=-\varepsilon(P+\lambda\sin\omega t),\quad \varepsilon<1,\quad \mathbf{u}=u\mathbf{e}_r+v\mathbf{e}_\theta+w\mathbf{e}_z,$$
$$u(-\varepsilon)=u(\varepsilon),\quad v(-\varepsilon)=v(\varepsilon),\quad w(-\varepsilon)=-w(\varepsilon). \tag{2}$$

D is the flow domain with the arbitrarily curved boundary ∂D, and ϕ and $\mathbf{S}$ represent the pulsating modified pressure field and the extra-stress tensor, respectively. The integral representation of the latter on the particle $\mathbf{X}$ of the fading memory fluid at the present time t,

$$\mathbf{S}=\mathbf{T}+\phi\mathbf{1}=\mathbf{F}_{s=0}^{\infty}[\mathbf{G}(\mathbf{X},s)],\quad s=t-\tau,$$

where τ represents the past time is based on the history $\mathbf{G}(\mathbf{X})$ of the strain on the particle and comes out of the Fréchet expansion of the extra-stress functional $\mathbf{F}$ in terms of the small parameter ε under the assumptions of isotropy, incompressibility and small strains,

$$\mathbf{S}(\mathbf{X},t;\varepsilon)=\varepsilon\mathbf{S}^{(1)}+\varepsilon^2\mathbf{S}^{(2)}+\mathrm{O}(\varepsilon^3). \tag{3}$$

The remaining variables are expanded into power series in ε pivoted around the rest state $\varepsilon=0$,

$$\mathbf{u}(\mathbf{X},\mathbf{t};\varepsilon)=\varepsilon\mathbf{u}^{(1)}(\mathbf{X},t)+\varepsilon^2\mathbf{u}^{(2)}(\mathbf{X},t)+\mathrm{O}(\varepsilon^3), \tag{4}$$

$$\phi(\mathbf{X},t;\varepsilon)=\varepsilon\phi^{(1)}(\mathbf{X},t)+\varepsilon^2\phi^{(2)}(\mathbf{X},t)+\mathrm{O}(\varepsilon^3), \tag{5}$$

where $n!(\cdot)^{(n)}$ refers to the nth-order partial derivative with respect to the perturbation parameter ε evaluated at $\varepsilon=0$,

$$n!(\cdot)^{(n)}=\left.\frac{\partial^n(\cdot)}{\partial\varepsilon^n}\right|_{\varepsilon=0}.$$

The integral forms of the Fréchet stresses $\mathbf{S}^{(i)}$ are developed and given elsewhere (Siginer, 1991a,b, 1992) up to and including third order. The first and second order Fréchet stresses read,

$$\mathbf{S}^{(1)}=\int_0^\infty G(s)\mathbf{A}_1^{(1)}(t-s)\,\mathrm{d}s, \tag{6}$$

$$\mathbf{S}^{(2)}=\int_0^\infty G(s)\mathbf{A}_1^{(2)}(t-s)\,\mathrm{d}s+\int_0^\infty G(s)\mathbf{L}_1(t-s)\,\mathrm{d}s+\int_0^\infty\int_0^\infty\gamma(s_1,s_2)\mathbf{A}_1^{(1)}(t-s_1)\mathbf{A}_1^{(1)}(t-s_2)\,\mathrm{d}s_1\,\mathrm{d}s_2, \tag{7}$$

$$\mathbf{A}_1^{(j)}(t-s) = 2\mathbf{D}\lfloor \mathbf{u}^{(j)}(\mathbf{X}, t-s)\rfloor, \quad j = 1, 2,$$

where $G(s)$ and $\gamma(s_1, s_2)$ refer to the shear relaxation and quadratic shear relaxation moduli, respectively, and the first Rivlin–Ericksen kinematic tensor $\mathbf{A}_1$ and its derivatives are defined in terms of the rate of deformation tensor $\mathbf{D}$ and its derivatives with respect to ε evaluated at $\varepsilon = 0$,

$$\begin{aligned} &\mathbf{A}_1 = \nabla\mathbf{u} + \nabla\mathbf{u}^{\mathrm{T}}, \quad \mathbf{A}_1^{(1)}(t-s) = \mathbf{A}_1\lfloor \mathbf{u}^{(1)}(\mathbf{x}, t-s)\rfloor, \\ &\mathbf{A}^{(j)}(t-s) = 2\mathbf{D}\lfloor \mathbf{u}^{(j)}(\mathbf{x}, t-s)\rfloor, \quad j = 1, 2. \end{aligned} \tag{8}$$

The tensor $\mathbf{L}$, is a function of $\mathbf{A}_1^{(j)}(t-s)$ and of the history integral ξ^* of the path of the particle $\mathbf{X}$ (Siginer, 1991a,b),

$$\mathbf{L}_1(t-s) = \xi^* \cdot \nabla\mathbf{A}_1^{(1)} + \mathbf{A}_1^{(1)}\nabla\xi^* + (\mathbf{A}_1^{(1)}\nabla\xi^*)^{\mathrm{T}}, \tag{9}$$

$$\xi^* = \int_t^\tau \mathbf{u}^{(1)}(\mathbf{X}, \tau')\,\mathrm{d}\tau', \quad t > \tau. \tag{10}$$

2.1. Longitudinal field

At the first order the Stokes problem is derived using (1)–(6) and reads as,

$$\rho\mathbf{u}_{,t}^{(1)} = -\nabla\phi^{(1)} + \nabla\cdot\mathbf{S}^{(1)}, \quad \nabla\cdot\mathbf{u}^{(1)} = 0, \quad \phi_{,z}^{(1)} = -(P + \lambda\sin\omega t), \quad \mathbf{u}^{(1)}\Big|_{\partial D_0} = 0, \quad \mathbf{u}^{(1)}(0, z) < \infty. \tag{11}$$

The first order velocity is unidirectional and is of the following form,

$$\mathbf{u}^{(1)} = w^{(1)}(r, \theta, t)\mathbf{e}_z.$$

The transversal velocity components u and v are of order $\mathrm{O}(\varepsilon^2)$. The mass conservation is identically satisfied at this order, and the linear momentum balance $(11)_1$ yields using (6) and (8),

$$\begin{aligned} &\rho w_{,t} = -(P + \lambda\sin\omega t) + \int_0^\infty G(s)\nabla^2 w(r, \theta, t-s)\,\mathrm{d}s \quad \text{at } \mathrm{O}(\varepsilon), \\ &\nabla^2 = \frac{\partial^2}{\partial r^2} + \frac{1}{r}\frac{\partial}{\partial r} + \frac{1}{r^2}\frac{\partial^2}{\partial\theta^2}, \end{aligned} \tag{12}$$

to be solved subject to,

$$w^{(1)}\Big|_{\partial D_0} = 0, \quad w(0, z, t) < \infty.$$

2.2. The transversal field

The second order problem is derived through the use of (2)–(5) and (1) and is defined by

$$\begin{aligned} &\rho\mathbf{u}_{,t}^{(2)} = -\nabla\phi^{(2)} + \nabla\cdot\mathbf{S}^{(2)}, \quad \nabla\cdot\mathbf{u}^{(2)} = 0 \quad \text{in } D_0, \\ &\mathbf{u}^{(2)}\Big|_{\partial D_0} = 0, \quad \mathbf{u}^{(2)}(0, \theta, z, t) < \infty. \end{aligned} \tag{13}$$

Both the longitudinal and transversal fields at the first and second orders, respectively, are defined and are to be solved in the rest state domain D_0 which is geometrically the same as the physical flow domain D.

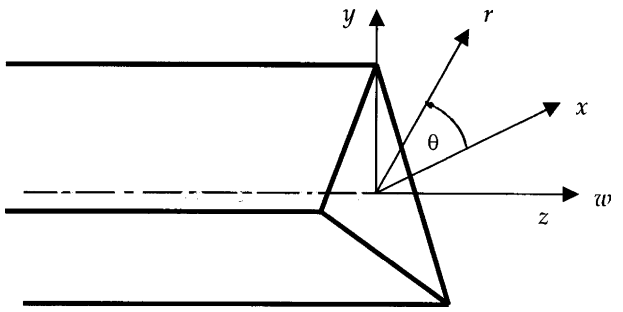

Fig. 1. Coordinate system in a straight tube of arbitrary cross-sections.

Both problems are set in the rest state domain as a mathematical requirement because the rest state as well as the constitutive structure are perturbed through the parameter ε in the driving pressure gradient. The basic system is described in Fig. 1.

2.3. Domain mapping

We further develop and use ideas due to Letelier and Leutheusser (1985) and Letelier et al. (1995), and postulate that the structure of the primary longitudinal flow in the deformed domain D at $O(\varepsilon)$ is given by

$$w = (R^2 - r^2 + \varepsilon_1 r^n \sin n\theta)\lfloor w_0(r,\theta,t) + \varepsilon_1 H_1(r,\theta,t) + \varepsilon_1^2 H_2(r,\theta,t) + O(\varepsilon_1^3)\rfloor, \quad \varepsilon_1 < 1, \tag{14}$$

where $w_0(r,\theta,t)$ refers to the longitudinal velocity field of the base flow, that is the velocity field in the unmapped domain $\overline{D}_0$ corresponding to flow in a tube with a known contour $\partial\overline{D}_0$. The contour ∂D of the new conduit is determined by the numerical values of the parameters (ε_1, n). Large deformations of the contour $\partial\overline{D}_0$ of the base flow are allowed by this mapping technique. The base flow w_0 in the conduit with the selected contour ∂D_0 is recovered as $\varepsilon_1 \to 0$, and the values of $0 < \varepsilon_1 < 1$, $n > 1$ give rise to a spectrum of tube contours. As an example the set $\varepsilon_1 = 0.22$, $n = 4$ corresponds to a square. The factored term in (14) is set to zero to satisfy the no-slip condition. The equation thus obtained is called the shape factor and generates a rich spectrum of shapes by varying (ε_1, n).

As $r^n \sin n\theta$ used in the representation (14) of the longitudinal velocity is part of the infinite set of homogeneous solutions of the Laplace equation one could as well have used $r^n \cos n\theta$ or $r^n(\cos n\theta + \sin n\theta)$. Therefore the representation (14) for the longitudinal velocity written in terms of $\sin n\theta$ is also valid with $\sin n\theta$ replaced with $\cos n\theta$ or $(\cos n\theta + \sin n\theta)$. It is also important to note that the parameter ε_1 in (14) is not dimensionless. Its dimension depends on the integer number n which in turn affects the dimension of the functions H_i, $i = 1, 2$, $[\varepsilon_1] = L^{2-n}$, $[H_1] = L^{n-3}T^{-1}$, $[H_2] = L^{2n-5}T^{-1}$ where L and T represent length and time, respectively.

2.4. Solution for the base flow w_0

A tube with circular contour $\partial\overline{D}_0$ is selected as the base flow. We note that the constitutive structure is perturbed through the parameter ε and the contour $\partial\overline{D}_0$ through ε_1 when n is selected. Thus at $O(\varepsilon, \varepsilon_1^0)$, that is in the circular tube, the problem reduces to that of solving (12) with $w^{(1)} \to w_0(R^2 - r^2)$ subject to $(R^2 - r^2)w_0 \mid_{\partial\overline{D}_0} = 0$. The solution is obtained in Siginer (1991a) by the second author and will be reproduced here,

$$w_0(r,t) = \frac{P}{4\mu} + \frac{2}{R^2 - r^2}\mathrm{Re}\left[A(r)\,\mathrm{e}^{\mathrm{i}\omega t}\right], \quad A(r) = \frac{\lambda}{2\rho\omega}\left[\frac{I_0(\Lambda r)}{I_0(\Lambda R)} - 1\right],$$
$$\Lambda^2 = \frac{\mathrm{i}\rho\omega}{\int_0^\infty G(s)\,\mathrm{e}^{-\mathrm{i}\omega s}\,\mathrm{d}s} = \frac{\mathrm{i}\rho\omega}{\eta^*}, \tag{15}$$

where η^* and I_0 represent the complex viscosity and the modified Bessel function of order zero, respectively. The complex viscosity is the material parameter which determines the stresses that are linear in the shear rate, and it has components η' and η'' corresponding to the linearly viscous and elastic properties of the liquid, respectively.

2.5. Solution for the primary longitudinal flow at the lowest order in ε

Expanding (14) in powers of ε_1 gives,

$$w = w_0(R^2 - r^2) + \sum_{j=1}^{\infty} \varepsilon_1^j w_j, \quad w_1 = w_0 r^n \sin n\theta + (R^2 - r^2)H_1,$$

$$w_j = H_{j-1} r^n \sin n\theta + (R^2 - r^2)H_j.$$

Using (12) we obtain the consecutive problems satisfied by w_j,

$$\rho w_{j,t} = \int_0^\infty G(s)\nabla^2 w_j(r,\theta,t-s)\,\mathrm{d}s, \quad j = 1,\ldots,\infty. \tag{16}$$

It is worthwhile to note that each component w_j is not zero on the boundary ∂D_0 but $w^{(1)}\big|_{\partial D_0} = 0$ as the no-slip boundary condition is already satisfied by the shape factor.

We structure the solution at order $\mathrm{O}(\varepsilon, \varepsilon_1)$ as

$$w_1 = \left\{\left[B(r)\,\mathrm{e}^{\mathrm{i}\omega t} + \overline{B}(r)\,\mathrm{e}^{-\mathrm{i}\omega t}\right] + Cr^n\right\}\sin n\theta.$$

The solution is developed in Letelier et al. (2002) and the details will not be reproduced here.

$$B(r) = KI_n(\Lambda r), \quad (\Lambda, K) \in C,$$

where Λ is defined in (15) and I_n represents the complex modified Bessel function of order n and the complex constant K is computed as

$$K = K_1 + \mathrm{i}K_2,$$

$$K_j = \frac{R^n\left[p_j(R)S_{n_1}(R) - (-1)^j p_{3-j}(R)S_{n_2}(R)\right]}{S_{n_1}^2(R) + S_{n_2}^2(R)}, \quad j = 1,2,$$

$$I_n(\Lambda R) = S_{n_1}(R) + \mathrm{i}S_{n_2}(R),$$

$$p_j(R) = \lim_{r\to R}\frac{a_j(r)}{R^2 - r^2},$$

$$A(r) = a_1 + \mathrm{i}a_2,$$

where $A(r)$ is defined in (15). At order $\mathrm{O}(\varepsilon, \varepsilon_1^2)$,

$$w_2 = f(r,t)r^n \sin^2 n\theta + (R^2 - r^2)H_2.$$

We postulate

$$w_2 = B_{21}(r)\,\mathrm{e}^{\mathrm{i}\omega t} + \overline{B}_{21}\,\mathrm{e}^{-\mathrm{i}\omega t} + [B_{22}(r)\,\mathrm{e}^{\mathrm{i}\omega t} + \overline{B}_{22}(r)\,\mathrm{e}^{-\mathrm{i}\omega t}]\cos 2n\theta$$

and derive the problems which define B_{21} and B_{22} through substitution in (16),

$$L^2 B_{21} = 0, \quad \left(L^2 - \frac{4n^2}{r^2}\right)B_{22} = 0, \quad L^2 = \frac{\partial^2}{\partial r^2} + \frac{1}{r}\frac{2}{\partial r} - \Lambda^2,$$

the solutions to which are developed in Letelier et al. (2002) and read as

$$B_{2j}(r) = K_{2j} I_{2n(j-1)}(\Lambda r), \quad K_{2j} \in C,\ j = 1, 2.$$

2.6. Solution for the transversal field at the lowest order in ε

The transversal field arises at order $\mathrm{O}(\varepsilon^2)$. The details of the derivation are developed in Siginer and Letelier (2002) and only the summary will be given here. The driving terms at this order are both time independent and time dependent of the type $\mathrm{e}^{ki\omega t}$, $k = 1, 2$. Therefore, the transversal field has a time-averaged mean part represented by a time-averaged stream function $\psi_m(r, \theta)$ and components $\psi_k(r, \theta)$ oscillating with frequencies ω and 2ω and has the form,

$$\begin{aligned} &\mathbf{u}^{(2)} = \operatorname{curl}\psi(r, \theta, t)\mathbf{e}_z, \\ &\psi(r, \theta, t) = \psi_m(r, \theta) + \lfloor \psi_k(r, \theta)\,\mathrm{e}^{ki\omega t} + \text{Conj.} \rfloor, \quad k = 1, 2. \end{aligned} \tag{17}$$

The mathematical problem which defines the mean field $\psi_m(r, \theta)$ is developed using (7), (13) and (17) and reads as

$$\begin{aligned} -\mu r \nabla^4 \psi_m = \int_0^\infty G(s)\{[\nabla \cdot \mathbf{L}_1]_{r,\theta} - [r\nabla \cdot \mathbf{L}_1]_{\theta,r}\}_m \,\mathrm{d}s + \int_0^\infty\int_0^\infty \gamma(s_1, s_2)\{[\nabla \cdot (\mathbf{A}_1(s_1)\mathbf{A}_1(s_2))]_{r,\theta} \\ - [r\nabla \cdot (\mathbf{A}_1(s_1)\mathbf{A}_1(s_2))]_{\theta,r}\}_m \,\mathrm{d}s_1\,\mathrm{d}s_2, \end{aligned}$$

where $\{\}_m$ refers to the time-averaged terms. The tensor $\mathbf{L}_1$ and the tensorial product $\mathbf{A}_1(s_1)\mathbf{A}_1(s_2)$ are computed using (8) and (9) and are given as

$$\mathbf{L}_1(t - s) = 2w_{,r}(t - s)\xi_{,r}\mathbf{e}_r \otimes \mathbf{e}_r + \frac{2}{r^2} w_{,\theta}(t - s)\xi_{,\theta}\mathbf{e}_\theta \otimes \mathbf{e}_\theta + \frac{1}{r}[w_{,r}(t - s)\xi_{,\theta} + w_{,\theta}(t - s)\xi_{,r}][\mathbf{e}_r \otimes \mathbf{e}_\theta + \mathbf{e}_\theta \otimes \mathbf{e}_r],$$

$$\begin{aligned} \mathbf{A}_1^{(1)}(t - s_1)\mathbf{A}_1^{(1)}(t - s_2) = w_{,r}(s_1)w_{,r}(s_2)\mathbf{e}_r \otimes \mathbf{e}_r + \frac{1}{r^2} w_{,\theta}(s_1)w_{,\theta}(s_2)\mathbf{e}_\theta \otimes \mathbf{e}_\theta \\ + \frac{1}{r}[w_{,r}(s_1)w_{,\theta}(s_2)\mathbf{e}_r \otimes \mathbf{e}_\theta + w_{,r}(s_2)w_{,\theta}(s_1)\mathbf{e}_\theta \otimes \mathbf{e}_r], \end{aligned}$$

together with ξ computed through (10),

$$\xi^* = \xi\mathbf{e}_z = \mathbf{e}_z.$$

We postulate that the mean stream function ψ_m is structured as

$$\psi_m = H^2(r, \theta) f(r, \theta) + \psi_0, \tag{18}$$

where ψ_0 is an arbitrary constant which may be set to zero for convenience and $H(r, \theta)$ is the shape factor,

$$H(r, \theta) = R^2 - r^2 + \varepsilon_1 r^n \sin n\theta.$$

The no-slip boundary condition is met by the above definition of ψ_m, and the unknown function $f(r,\theta)$ is assumed to have the following form,

$$f(r,\theta) = \sum_{j=1}^{\infty} \varepsilon_1^j f_j(r,\theta).$$

Expanding the mean stream function ψ_m in a series we obtain,

$$\psi_m(r,\theta) = \varepsilon_1\psi_1 + \varepsilon_1^2\psi_2 + \mathrm{O}(\varepsilon_1^3),$$
$$\psi_m(r,\theta) = \varepsilon_1(R^2-r^2)^2 f_1(r,\theta) + \varepsilon_1^2[(R^2-r^2)^2 f_2(r,\theta) + 2(R^2-r^2)r^n \sin n\theta f_1(r,\theta)] + \mathrm{O}(\varepsilon_1^3).$$

Then the secondary flow is defined at the leading orders in ε_1 by

$$\mathrm{O}(\varepsilon^2,\varepsilon_1) : r\nabla^4\psi_1 = r\nabla^4\lfloor(R^2-r^2)^2 f_1(r,\theta)\rfloor,$$

$$\mathrm{O}(\varepsilon^2,\varepsilon_1^2) : r\nabla^4\psi_2 = r\nabla^4\lfloor(R^2-r^2)^2 f_2(r,\theta) + 2(R^2-r^2)r^n \sin n\theta f_1(r,\theta)\rfloor.$$

The full solution of the last two problems are given in Siginer and Letelier (2002) and the reader is referred to that work for details.

3. Discussion

Explicit computation of the longitudinal and transversal flow fields at the lowest orders using the equations developed depends on defining the material functions entering the field equations. The primary field in the longitudinal direction is framed in terms of the shear relaxation modulus $G(s)$ related to the complex viscosity η^*

$$\eta^* = \eta' - \mathrm{i}\eta'' = \int_0^{\infty} G(s)\,\mathrm{e}^{-\mathrm{i}\omega s}\,\mathrm{d}s.$$

We use an expression for $G(s)$ previously introduced by Siginer (1991a,b)

$$G(s) = \frac{k^k\mu}{\theta^k\Gamma(k)} s^{k-1}\,\mathrm{e}^{-ks/\theta}, \quad \theta = -\frac{\alpha_1}{\mu},\ 0 < k < 1,$$

where α_1 an μ are the first Rivlin–Ericksen constant—a material parameter—and the zero shear viscosity, and θ and k can be thought of as the natural time of the fluid and an adjustable parameter to bring the curve represented by the above definition of $G(s)$ for a given fluid (α_1 and μ_0 consequently are fixed and determined from separate experiments for the fluid under consideration) to better agreement with experimental data. This explicit representation of $G(s)$ meets the conditions for the stability of the rest state, that is $G(s) > 0$, $G'(s) < 0$, $G''(s) > 0$ and $G(s) \to 0$ as $s \to \infty$ which implies that the stress vanishes when the fluid is at rest. The first Rivlin–Ericksen coefficient is related to the first normal stress difference through,

$$\alpha_1 = -\int_0^{\infty} sG(s)\,\mathrm{d}s = -\lim_{\kappa\to 0}\frac{T_{zz}-T_{rr}}{2\kappa^2} = -\lim_{\kappa\to 0}\frac{N_1(\kappa^2)}{2\kappa^2}, \quad N_1(\kappa^2) > 0, \tag{19}$$

where T_{zz}, T_{rr} and κ represent the stress components in the longitudinal and radial directions and the shear rate, respectively. Thus the definition of the natural time θ of the fluid in terms of α_1 and a characteristic viscosity makes sense and is physically meaningful. In Figs. 2 and 3 we present the longitudinal field for a commercially available specific fluid and for large amplitude forcing. If the analysis is conducted up to and including fourth order in ε, then the present analysis is applicable to solutions of high-molecular weight polymers such as polyacrylamide in water.

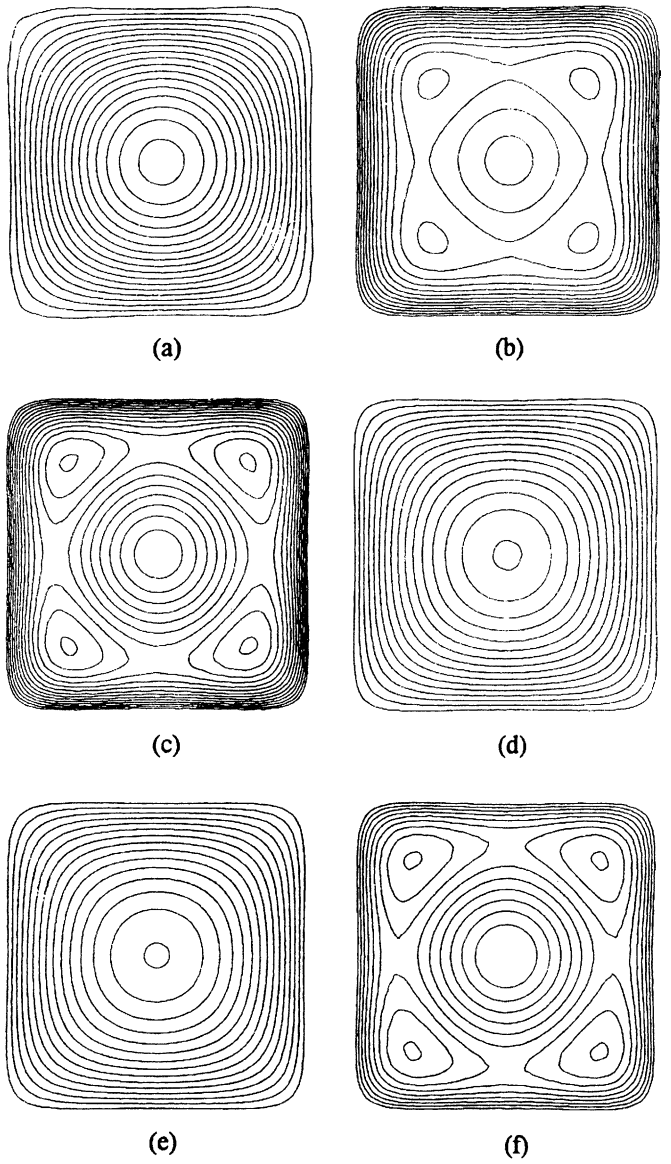

Fig. 2. Dimensionless axial velocity contours in a straight pipe of very approximately square cross-sectional shape ($n = 4, \varepsilon_1 = 0.22$) in the case of the large amplitude oscillation of the pressure gradient for increasingly elastic liquids starting with the linear Newtonian fluid ($\kappa = 0$). The amplitude λ of the pressure wave is equal to the mean gradient P, $\lambda/P = 1$. The non-dimensional velocity w^* and time t^* are defined as $w^* = w/W_0$ and $t^* = \omega t$ where $W_0 = PR^2/4\mu$, and other data is taken as $\omega = 10$ rad/s, $\rho = 0.89$ g/cm^3, $\mu = 200$ Poise, $\alpha_1 = -50$ g/cm, $R = 3$ cm. In the following Δ defines the dimensionless increment between axial velocity contours: (a) $\kappa = 0.0$, $t^* = 0.48\pi$, $\Delta = 2 \times 10^{-4}$; (b) $\kappa = 0.01$, $t^* = 0.365\pi$, $\Delta = 35 \times 10^{-5}$; (c) $\kappa = 0.5$, $t^* = 1.907\pi$, $\Delta = 10^{-3}$; (d) $\kappa = 0.5$, $t^* = 5\pi/4$, $\Delta = 0.2$; (e) $\kappa = 0.5$, $t^* = \pi/4$, $\Delta = 0.07$; (f) $\kappa = 1.0$, $t^* = 0.455\pi$, $\Delta = 36 \times 10^{-4}$.

In Fig. 3 longitudinal velocity profiles in both the shorter and longer cross-section semi-axes are shown for times associated to Fig. 1a and b.

For the computation of the transversal flows an explicit definition of the quadratic shear relaxation modulus $\gamma(s_1, s_2)$ is required in addition to the definition of the shear relaxation modulus $G(s)$. We note that

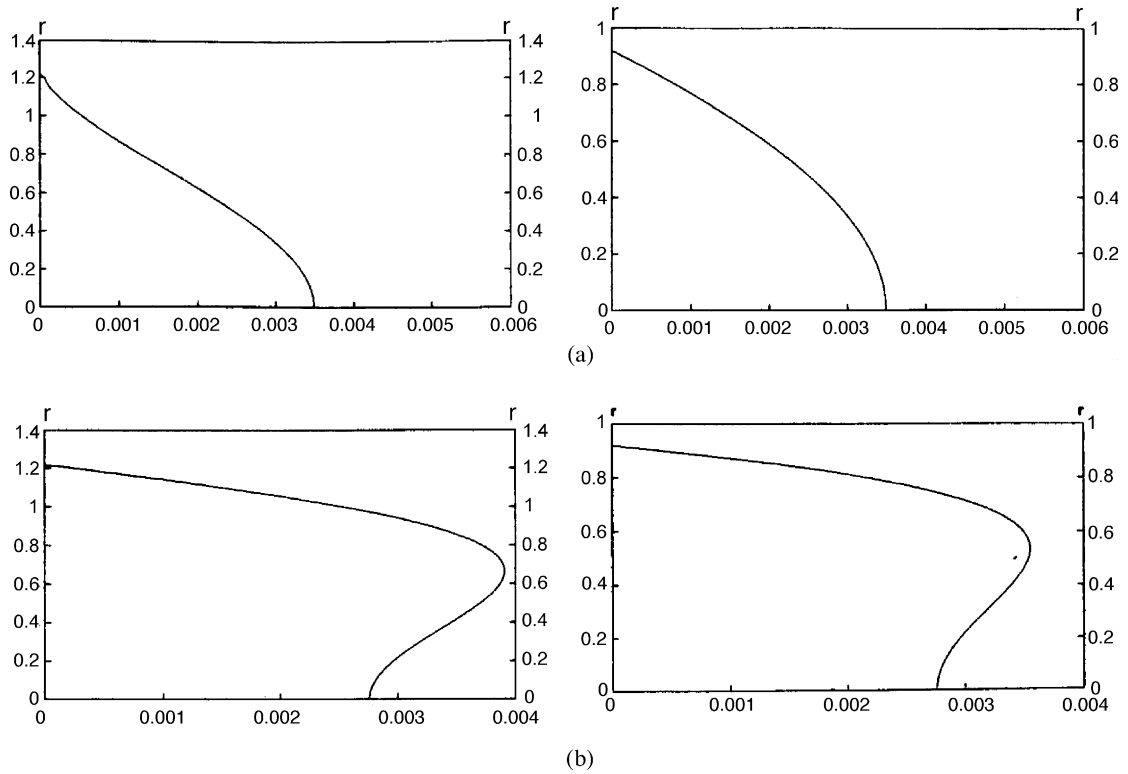

Fig. 3. Dimensionless velocity profiles in a square pipe ($n = 4, \varepsilon_1 = 0.22$) along the diagonal and the axis of the square in cases (a) and (b) in Fig. 1. There is one-to-one correspondence between Figs. 1 and 2. Thus case (a) in Fig. 1 corresponds to case (a) in Fig. 2. Length scale is R. Non-dimensional velocity is the same as in Fig. 2. The velocity profiles with the larger ordinate are obviously along the diagonal.

the quadratic shear relaxation modulus is related to both the first and second normal stress differences $N_1(\kappa^2)$ and $N_2(\kappa^2)$, respectively, through the second Rivlin–Ericksen constant α_2,

$$\int_0^\infty\int_0^\infty \gamma(s_1,s_2)\,\mathrm{d}s_1\,\mathrm{d}s_2 = -\alpha_2 = \lim_{\kappa\to 0}\frac{N_1(\kappa^2)+N_2(\kappa^2)}{\kappa^2}, \quad N_2(\kappa^2) = T_{rr} - T_{\theta\theta}. \tag{20}$$

The relationships (19) and (20) hold independently of the explicit representations adopted for $G(s)$ and $\gamma(s_1,s_2)$. In addition to these two material functions the driving terms in the field equations for the secondary flow depend on $\hat{\alpha}_2(\omega)$ the counterpart of α_2 for oscillatory motions,

$$\lim_{\omega\to 0}\hat{\alpha}_2(\omega) = \alpha_2, \quad \hat{\alpha}_2(\omega) = \int_0^\infty\int_0^\infty \gamma(s_1,s_2)\cos\omega(s_1,s_2)\,\mathrm{d}s_1\,\mathrm{d}s_2.$$

The second normal stress difference for oscillatory flows is given by

$$\hat{N}_2(\omega) = -\eta''(\omega)/\omega + \hat{\alpha}_2(\omega).$$

This expression collapses on to the second normal stress function $N_2(\kappa^2)$ for viscometric flows as $\omega \to 0$.

$$\lim_{\omega\to 0}\hat{N}_2(\omega) = \lim_{\kappa\to 0}\frac{N_2(\kappa^2)}{\kappa^2} = 2\alpha_1 + \alpha_2.$$

We adopt an expression previously used by Siginer (1991a,b), for $\gamma(s_1, s_2)$

$$\gamma(s_1, s_2) = \alpha_2 \sum_i^N C_{1i} l_i^2 \, \mathrm{e}^{-1_i(s_1+s_2)}, \quad \sum_i^N C_{1i} = 1, \tag{21}$$

which represents $\gamma(s_1, s_2)$ as a series in terms of the second Rivlin–Ericksen constant $\alpha_2 > 0$ and a discrete spectrum of relaxation times l_i^{-1}, $i = 1, \ldots, N$. This choice for the representation of $\gamma(s_1, s_2)$ satisfies (20). We compute,

$$\hat{\alpha}_2(\omega) = 2\alpha_2 \sum_j^N C_{1j} l_j^2 \frac{(l_j^2 - \omega^2)}{(l_j^2 + \omega^2)}.$$

It has been determined experimentally that, for the same commercially available fluid whose properties we use in this paper to obtain specific examples of the longitudinal velocity profiles and mean transversal streamline patterns, in small amplitude oscillatory rod climbing experiments a good fit with experimental data is obtained when $\omega < 20$ rad/s if $N = 2$ and

$$l_1 = 3.8079 \text{ s}^{-1}, \quad l_2 = 17.5214 \text{ s}^{-1},$$

$$c_1 = 0.9735, \quad c_2 = 1 - 0.935.$$

We adopt the hypothesis that (21) represents the behavior of this specific fluid in all periodic motions which perturb the rest state when $\omega < 20$ rad/s, and we present in Figs. 3 and 4 examples of the mean secondary flow streamline patterns.

Figs. 2 and 3 represent snapshots from the evolution in time of the axial field of a real fluid in straight tubes of very approximately square cross-section, in the case of large amplitude forcing. Fig. 2 shows the isovels for a very approximately square ($n = 4, \varepsilon_1 = 0.22$) cross-section for different values of the power index κ at different times during a period. When the index is zero the flow is Newtonian. Figs. 2a and 3a represent this linear case at particular times during the evolution of the field in a period. In the remaining figures as the value of the power index κ increases the loss and storage moduli $\omega\eta'$ and $\omega\eta''$ decrease and increase, respectively, at fixed frequency, that is the apparent viscosity decreases and the elastic effects increase. Maximum velocities in the positive z direction are much larger than those in the negative direction, thus there is a net flow in the positive direction equal to the Newtonian flow rate under the same pulsating gradient. That is because the time-averaged velocity profile over a period of the linearly viscoelastic fluid is the same as that of the Newtonian fluid with the same zero-shear viscosity.

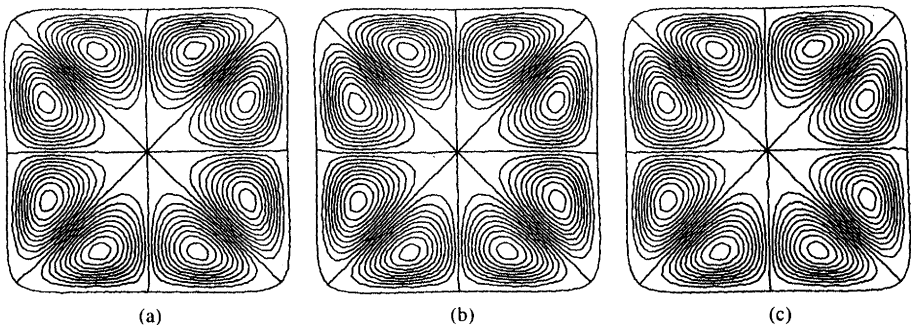

Fig. 4. Dimensionless mean secondary flow streamline plots in a square tube ($n = 4, \varepsilon_1 = 0.22$) when the amplitude λ of the oscillation of the pressure gradient is of the same order of magnitude as the mean gradient P, $\lambda/P = 1$, and for increasingly elastic liquids. The data and definitions are the same as in Fig. 1. Particles move towards the corners along the walls. $|\Delta\Psi_m| = 0.1 \times |\Psi_m|_{\max}$: (a) $\kappa = 0.01$, $|\Psi_m|_{\max} = 1.29 \times 10^{-8}$; (b) $\kappa = 0.5$, $|\Psi_m|_{\max} = 2.3 \times 10^{-4}$; (c) $\kappa = 1.0$, $|\Psi_m|_{\max} = 4.4 \times 10^{-4}$.

The Womersley number which represents the ratio of the inertial forces to viscous forces in oscillatory flows is defined as

$$W_0 = \sqrt{\frac{\rho\omega}{\mu}}R.$$

The Deborah number is the inverse of the ratio of the characteristic process time to the natural time (the largest relaxation time) of the fluid,

$$De = \frac{\theta}{t_0}$$

and the Weissenberg number which governs the magnitude of the elastic reaction of the fluid under the particular process conditions is framed as

$$We = \theta\kappa,$$

where κ denotes a representative shear rate of the process.

With Newtonian fluids, in the case of large Womersley numbers, inertial forces are particularly dominant close to the wall where the velocity gradient shows large fluctuations with r at any given time during a period, and close to the centerline the velocity profile would look more like that of the plug flow. By contrast, for small and moderate Womersley numbers, viscous forces dominate and velocity gradient fluctuations close to the wall are completely smoothed out. In the cases presented in this paper the W_0 number is small and the fluid behaves very much like a linear fluid. When the De number is smaller than unity the process time, that is the period, is longer than the natural relaxation time of the fluid and the particle at a fixed location has time to react. The magnitude of this reaction depends on the We number. Thus for $De < 1$ and ω moderate the fluid reacts quite differently depending on the value of the We number. For small amplitude oscillations We is about forty times smaller than for large amplitude oscillations. In the latter case the velocity profiles may present maxima and inflexion points at a fixed time in a period, where as in the former the velocity shows a smooth increase from the wall to the centerline at all times in a period with small departures from Newtonian behavior.

Figs. 4 and 5 represent the secondary flow structure in a square cross-section at increasing values of the power index κ and snapshots of the development of the secondary flows as the circular cross-section is continuously deformed to yield the square shape, respectively. We note that the strength of the secondary flow increases by more than three orders of magnitude as the linear elasticity of the fluid increases from

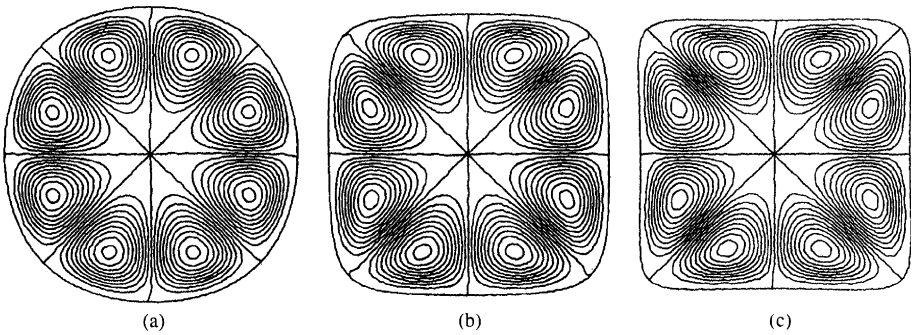

Fig. 5. Snapshots of the evolution of the mean secondary flow field at various values of ε_1 and fixed $\kappa = 0.5$ as the circular tube is continuously deformed by varying ε_1 to culminate in the square tube ($n = 4, \varepsilon_1 = 0.22$). $|\Delta\Psi_m| = 0.1 \times |\Psi_m|_{\max}$: (a) $n = 4$, $\varepsilon_1 = 0.044$, $|\Psi_m|_{\max} = 6.1 \times 10^{-7}$; (b) $n = 4$, $\varepsilon_1 = 0.176$, $|\Psi_m|_{\max} = 1.8 \times 10^{-5}$; (c) $n = 4$, $\varepsilon_1 = 0.22$, $|\Psi_m|_{\max} = 2.3 \times 10^{-4}$.

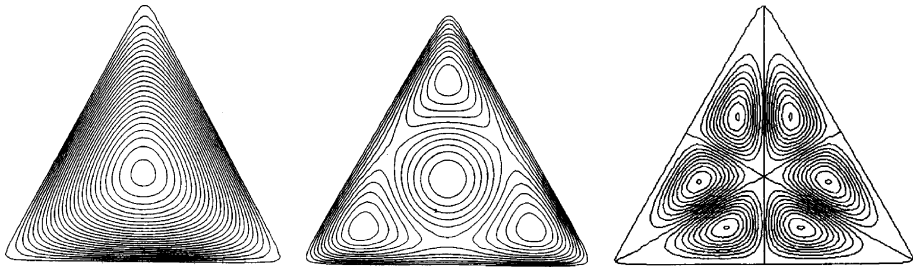

Fig. 6. Dimensionless axial velocity contours in a straight pipe of very approximately triangular cross-sectional shape: (a) $\kappa = 0.0$, $t^* = 0.25\pi$; (b) $\kappa = 0.5$, $t^* = 1.907\pi$; (c) characteristic dimensionless mean secondary flow streamline plots.

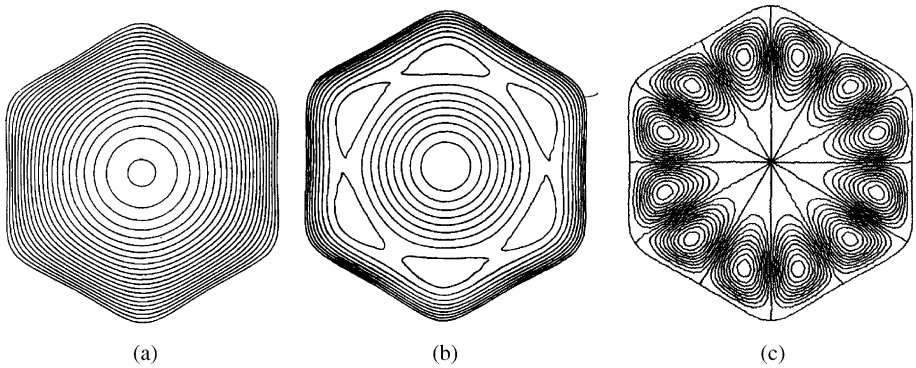

Fig. 7. Dimensionless axial velocity contours in a straight pipe of very approximately hexagonal cross-sectional shape: (a) $\kappa = 0.0$, $t^* = 0.48\pi$; (b) $\kappa = 1.0$, $t^* = 0.455\pi$; (c) characteristic dimensionless mean secondary flow streamline plots.

almost Newtonian ($\kappa \sim 0$) to $\kappa = 1$. This is a natural trend coming from the structure of the relaxation modulus G.

The number of vortices in a cross-section is always twice the number of the straight sides of the contour. The latter is equal to the parameter n in the shape factor. The vortices are symmetrical with respect to all the symmetry lines that can be drawn in any given cross-sectional shape. The order of magnitude of the strength of the secondary flows can be determined from dimensional analysis considerations as shown by Pipkin (1965). The strength of the secondary flow in terms of the transverse velocity is of the order We^3 compared to the longitudinal velocity.

In Figs. 6 and 7 we further show corresponding results of longitudinal and transversal fields descriptions for triangular and hexagonal shapes.

4. Conclusion

Longitudinal and transversal flow field of Green–Rivlin fluids in straight tubes of arbitrary cross-sections have been determined for the case of a pulsating pressure gradient. Results show consistent flow patterns for a variety of shapes, and for different values of the relevant fluid, and flow parameters.

Many relevant results, mainly of a kinematic nature, come out from the structure of (18), in which the shape factor $H(r, \theta)$ can be conveniently specified, through parameters ε_1, and n so that it describes a wide

arrange of cross-sectional shapes. The parameter ε_1 is intrinsically small, its maximum allowable value decreasing as n increases. These conditions are replicated in like analysis of other viscoelastic fluids, such as those described by the Phan-Thien–Tanner model, especially for steady flow in non-circular pipes. In such cases, a transversal stream function of similar structure to (18) can be found (Letelier et al., 2001), in which parameters ε_1 and n play the same role as in (18).

Previous comments allow us to state that the kinematic structure of secondary flows, as shown in Figs. 4, 6 and 7 are common to some viscoelastic flows. This statement is further backed by numerical results found by Xue et al. (1995) in their study of secondary flows of Phan-Thien–Tanner fluids in rectangular pipes. The strength of these flows is however, dependent on the values of the physical parameters associated to each constitutive fluid model.

Acknowledgement

The support of the Chilean Fund for Scientific and Technological Research (FONDECYT) through Grants 1970810, 1010173 and 7010173 is gratefully acknowledged.

References

Barnes, H.A., Townsend, P., Walters, P., 1971. On pulsatile flow of non-Newtonian liquids. Rheol. Acta 10, 517–527.

Fosdick, R.L., Serrin, J., 1973. Rectilinear steady flow of simple fluid. Proc. R. Soc. London A 332, 311–333.

Gao, S.X., Hartnett, J.P., 1993. Steady flow of non-Newtonian fluids through rectangular ducts. Int. Commun. Heat Mass Transfer 20, 197–210.

Gao, S.X., Hartnett, J.P., 1996. Heat transfer behavior of Reiner–Rivlin fluids in rectangular ducts. Int. J. Heat Mass Transfer 39, 1317–1324.

Hartnett, J.P., Kostic, M., 1985. Heat transfer to a viscoelastic fluid in laminar flow through a rectangular channel. Int. J. Heat Mass Transfer 28, 1147–1155.

Hartnett, J.P., Kostic, M., 1989. Heat transfer to Newtonian and non-Newtonian fluids in rectangular ducts. Adv. Heat Transfer 19, 247–355.

Letelier, M.F., Leutheusser, H.J., 1985. Laminar flow in conduits of unconventional shape. J. Eng. Mech. 111 (6), 768–776.

Letelier, M.L., Leutheusser, H.J., Márquez, G., 1995. Laminar fluid transients in conduits of arbitrary cross-section. J. Eng. Mech. 121, 1069–1074.

Letelier, M.F., Olguín, M.A., Siginer, D.A., 2001. Steady secondary flows of Phan-Thien–Tanner fluids in pipes of complex shapes. In: Proceeding of the 2001 ASME International Mechanical Engineering Congress and Exposition, Rheology and Fluid Mechanics of Nonlinear Material, IMECE 2001/FED-24909, New York.

Letelier, M.F., Siginer, D.A., Cáceres, C., 2002. Pulsating flow of viscoelastic fluids in straight tubes of arbitrary cross-section, Part I: Longitudinal field. Int. J. Non-Linear Mech. 37, 369–393.

Nikuradse, J., 1930. Turbulente stromung in Nicht-Kreisformigen Rohren. Ingenieur Arch. 1, 306–332.

Oldroyd, J.G., 1965. Some steady flows of the general elastico-viscous liquids. Proc. R. Soc. London A 283, 115–133.

Pipkin, A.C., 1965. Proceedings of the Fourth International Congress on Rheology, vol. I. Wiley-Interscience, New York, pp. 213–222.

Siginer, D.A., 1991a. Oscillating flow of a simple fluid in a pipe. Int. J. Eng. Sci. 29 (12), 1557–1567.

Siginer, D.A., 1991b. On the pulsating pressure gradient driven flow of viscoelastic liquids. J. Rheol. 35, 271–312.

Siginer, D.A., 1992. On the effect of boundary vibration on Poiseuille flow of an elastico-viscous liquid. J. Fluids Struct. 6, 719–748.

Siginer, D.A., Valenzuela-Rendón, A., 1993. Energy considerations in the flow enhancement of viscoelastic liquids. J. Appl. Mech. 60, 344–351.

Siginer, D.A., Letelier, M.F., 2002. Pulsating flow of viscoelastic fluids in straight tubes of arbitrary cross-section, Part II: Secondary flows. Int. J. Non-Linear Mech. 37, 395–407.

Xue, S.C., Phan-Thien, N., Tanner, R.I., 1995. Numerical study of secondary flows of viscoelastic fluid in straight pipes by an implicit volume method. J. Non-Newton. Fluid Mech. 59, 191–213.

Mario F. Letelier is full Professor at the Department of Mechanical Engineering of the University of Santiago of Chile. He is also Director of the Center for Research in Creativity and Higher Education. His main areas of research and scholarship are Non-Newtonian Fluid Mechanics, Heat Transfer and also Institutional Analysis.

Dennis A. Siginer is Professor of the College of Engineering at Wichita State University. He has been actively engaged with the Fluids Engineering. He has organized several symposia on Rheology, Non-linear Materials and related subjects. His main areas of research are Non-Newtonian Fluid Mechanics and Rheology.